Eur Biophys J (2001) 30: 284–294
DOI 10.1007/s002490100135

ARTICLE

Wolfgang Feneberg · Monika Westphal
Erich Sackmann

Dictyostelium cells' cytoplasm as an active viscoplastic body

Received: 12 October 2000 / Revised version: 14 December 2000 / Accepted: 15 December 2000 / Published online: 21 April 2001

Abstract We applied a recently developed microrheology technique based on colloidal magnetic tweezers to measure local viscoelastic moduli and active forces in cells of *Dictyostelium discoideum*. The active transport of nonmagnetic beads taken up by phagocytosis was analyzed by single particle tracking, which allowed us to measure the length of straight steps and the corresponding velocities of the movements. The motion consists of a superposition of nearly straight long-range steps (step length in the micrometer range) and local random walks (step widths about 0.1 μm). The velocities for the former type of motion range from 1 to 3 μm/s. They decrease with increasing bead size and are attributed to rapid active transport along microtubuli. The short-range local motions exhibit velocities of less than 0.5 μm/s and reflect the internal dynamics of the cytoplasm. Viscoelastic response curves were measured by application of force pulses with amplitudes varying between 50 pN and 400 pN. Analysis of the response curves in terms of mechanical equivalent circuits yielded cytoplasmic viscosities varying between 10 and 350 Pa s. Simultaneous analysis of the response curves and of the bead trajectories showed that the motion of the beads is determined by the local yield stress within the cytoplasmic scaffold and cisternae, which varies between $\sigma = 30$ Pa and 250 Pa. The motion of intracellular particles is interpreted in terms of viscoplastic behavior and the apparent viscosity is a measure of the reciprocal rate of bond breakage within the cytoplasmatic network. The viscoelastic moduli are interpreted as dynamic quantities which depend sensitively on the amplitude of the forces, and the rate of bond breakage is determined by the Arrhenius-Kramers law with the activation energy being reduced by the work performed by the applied force. In agreement with previous work, we provide evidence that the myosin II-deficient cells exhibit higher yield stresses, suggesting that the function of myosin II as a cross-linker is taken over by the other (non-active) cross-linkers.

Keywords Magnetic tweezers · *Dictyostelium discoideum* · Viscoelasticity · Rheology

W. Feneberg · E. Sackmann (✉)
Fakultät für Physik, Lehrstuhl für Biophysik,
E22, Technische Universität München,
James-Franck-Strasse, 85747 Garching, Germany
E-mail: sackmann@physik.tu-muenchen.de
Tel.: +49-089-28912472
Fax: +49-089-28912469

M. Westphal
MPI für Biochemie, 82152 Martinsried, Germany

Introduction

Our knowledge of the biochemical basis of cell signaling or intracellular trafficking has been advanced greatly over recent years (e.g. Alberts et al. 1994; Pawson and Scott 1997; Small et al. 1999). However, little is known about the control of the microscopic structure and the physical properties of the cell membrane and the cytoskeleton mediated through the activation of second messengers or enzyme cascades. One reason is the lack of microscopic techniques enabling real time measurements of local structural and physical properties of cells.

One way to characterize local structural changes in cell cytoplasm is micro-fluorescence combined with immunostaining or labeling of cellular constituents with green fluorescence protein (GFP). A more physical approach is to characterize the local structure of cells through viscoelastic parameters such as the elastic storage modulus and the shear viscosity (Kolodney and Elson 1993; Ziemann et al. 1994). This approach provides a physical tool to study structure-function relationships in cells since many cellular processes regulated by cell signaling such as shape changes, locomotion, or cell adhesion depend on the viscoelastic properties of both the membrane and the cytoskeleton (Janmey 1995; Raucher et al. 2000). For this purpose we developed a magnetic bead micro-rheometer enabling local measurements of the viscoelastic moduli of both the membrane and the cytoskeleton (Ziemann et al. 1994; Bausch et al. 1998,

1999). It enables the application of forces up to 10 nN and is thus complementary to the established optical tweezers technique. By functionalizing the beads with specific ligands (such as fibronectin), specific entities of the cell (such as integrins and the associated intracellular actin cortex) can be probed. In addition, this technique allows measurements of the local transport forces within the cell. Two types of experiments can be performed: measurements of viscoelastic response curves and magnetophoresis. In the former case, the time-dependent deflection of the beads following a large magnetic force pulse is measured by high-resolution particle tracking. In the latter case, the motion of the bead subjected to a small constant force is followed (Bausch et al. 1999).

In order to determine the viscoelastic moduli of cells from response curves, one would have to calculate the local elastic and viscous stresses and strains. This would require, however, knowledge about the structural features of the bead environment in order to apply the viscoelastic theory in a rigorous way. Fortunately, quantitative information on the local elastic and viscous properties of the environment of the micro-probe can be gained by analyzing its force-induced motion in terms of a simple mechanical equivalent circuit composed of suitable arrays of springs and dashpots. The local viscoelasticity is thus characterized in terms of an effective spring constant μ and an effective viscosity η. The advantage of magnetic bead rheology is the possibility to repeat measurements with a single colloidal probe at different sites within one cell. In this way it was shown that the cytoplasm of macrophages exhibits a pronounced viscoelastic heterogeneousness, resulting in a large variability of the elastic modulus ($\mu \approx 20$–700 Pa), whereas the viscosity varies less strongly ($\eta \approx 70$–350 Pa s).

In the present work we first studied the intracellular transport of colloidal beads internalized by phagocytosis. We measured the effective viscoelastic moduli of the cytoplasm by magnetic bead micro-rheometry and attempted to measure the active forces mediating the transport of phagosomes containing the magnetic beads (in the following called *magnetosomes*). The active motion of the beads consists of nearly straight paths of 1–3 μm length which are interrupted by local random walks with step-widths of the order of 100 nm. In order to determine velocity distributions of this quasi-random walk, the length of the quasi-straight paths was analyzed by using a method introduced by de Win et al. (1999). Comparison of the velocity distributions of wild-type cells and myosin II-null mutants shows that removal of myosin II shifts the velocity distribution towards lower values, suggesting that the apparent mechanical strength of the cytoplasm is increased compared to wild-type cells, confirming previous micropipette studies (Merkel et al. 2000).

In the second part of this paper the viscoelasticity of the cytoplasm is studied by magnetic bead micro-rheometry described elsewhere (e.g. Bausch et al. 1998). The viscoelastic response curves induced by force pulses with amplitudes between 50 pN and 400 pN and the associated bead trajectories were evaluated. The viscoelastic response depends drastically on the applied magnetic force F_{mag}. At forces $F_{mag} = 400$ pN the beads move in nearly all cases along straight lines. At forces between $F_{mag} = 100$ pN and 200 pN the paths of the deflected beads exhibit often sharp bends, which are attributed to bead deflection by obstacles which cannot be penetrated at these forces. The response curves for $F_{mag} = 140$ pN, 200 pN, and 400 pN were formally analyzed in terms of a simple mechanical equivalent circuit, yielding effective viscosities varying between 20 and 100 Pa s. At $F_{mag} < 100$ pN the beads are only occasionally deflected after a delay time of several seconds, while their motion consists mostly of local random walks.

The strong force dependence can be understood by assuming that the cytoplasm is a highly heterogeneous viscoplastic network (Neuhäuser and Schwink 1993). Therefore the local mechanical strength of the cytoplasm is characterized in terms of the yield stress varying between 30 Pa and 250 Pa. The bead velocity is thus determined by the rate of bond breakage within the cytoplasmic network and η is an effective viscosity which is inversely proportional to this rate. The rate of local bond dissociation is expected to be a thermally excited process which is accelerated by the external force according to the Arrhenius-Kramers theory. The force induced shear rate γ is related to the local stress σ according to:

$$\dot{\gamma} = \gamma_0 \exp\left[-\frac{\Delta G(T)}{k_B T}\right] \quad (1)$$

with $\Delta G = G_0 - \sigma V$. V is the so-called activation volume and σV is thus a measure for the work performed by the external force to advance the bead by a step of the order of the mesh size. Such equations are also used to describe the behavior of viscoplastic technical materials, e.g. glasses (Neuhäuser and Schwink 1993). Owing to the intrinsic probability of bond breakage, the shear rate is a dynamic quantity which depends on the rate at which the external stress is applied.

In the above viscoplastic image of the cytoplasm the transition between fast long-range and the localized random motion of the magnetosomes can also be explained in terms of the large variability of the mechanical strength. Since we found that the active force F_{act} produced by the cell itself is about 100 pN, it cannot rapidly transport the beads through the regions of high yield stress corresponding to about 60 Pa. The permeation velocity in the direction of the active force is slowed down since the motion is determined by the rate of bond breakage following Eq. (1). We estimated the active forces in the cytoplasm by analyzing the changes of the bead velocities immediately after application of force pulses.

Materials and methods

The magnetic tweezers

The micro-rheometer resembles the experimental set-up described previously (Ziemann et al. 1994; Schmidt et al. 1996; Bausch et al.

1998). The set-up used in the present paper is shown in Fig. 1a. The central measuring unit consists of a sample holder and a magnetic coil with 1200 turns of 0.7 mm diameter copper wire. The sample holder with dimensions 50×55×50 mm^3 is mounted on an AXIOVERT 10 microscope (Zeiss, Oberkochen, Germany). The coil current is produced by a voltage-controlled current supply built in the authors' laboratory that transforms the voltage signal of a FG 9000 function generator (ELV, Leer, Germany) in a current signal with amplitudes of up to 4 A. The microscope image is recorded by a CCD camera (C3077, Hamamatsu Photonics, Hamamatsu City, Japan) connected to a VCR (WJ-MX30, Matsushita Electric, Osaka, Japan). The recorded sequences are digitized using an Apple Power Macintosh 9500 (Apple Computer, Cupertino, Calif., USA) equipped with a LG3 frame grabber card (Scion, Frederick, Md., USA). The position of the particles is determined with an accuracy of about 10 nm using a self-written single-particle tracking algorithm implemented in the public domain image processing software NIH Image (National Institutes of Health, Bethesda, Md., USA).

Cell preparation

Mutant and wild-type cells of *Dictyostelium discoideum* were cultivated on a petri dish in liquid nutrition medium (''Standardnährlösung'', Max-Planck-Institut für Biochemie, Martinsried, Germany). Wild-type AX2 and myosin II-null mutant HS2205 (Manstein et al. 1989) were both transfected to express GFP-tagged α-tubulin (cell lines HG1668 and HG1671, Neujahr et al. 1998). For each experiment, cells were taken from axenic culture. To starve the cells they were separated from the nutrient by washing and centrifuging three times in cold 17 mM K-Na phosphate buffer, pH 6.0. After each centrifugation step the supernatant was discarded and the cells were resuspended in phosphate buffer at 4 °C by vortexing. Experiments were performed no longer than 2 h after the final washing step.

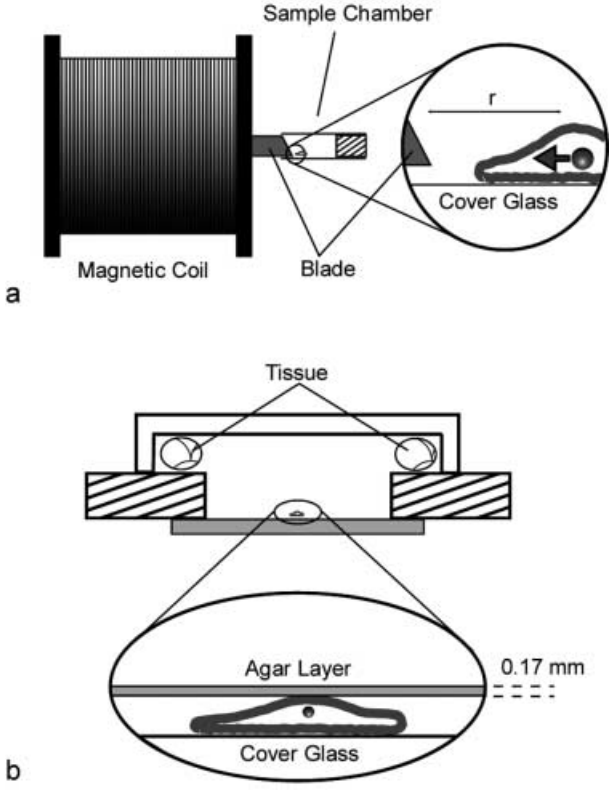

Fig. 1 **a** Set-up of the magnetic tweezers. **b** Illustration of the measuring chamber and flattening of *Dictyostelium* by pressing a 0.17 mm thick agar layer over adherent cells. The measuring chamber is closed by deposition of a flat petri dish over the measuring chamber. To avoid drying out of the cells and agar layer, a wet tissue is assembled around the circumference of the measuring chamber

Colloidal probes

Three types of colloidal probes were used: (1) carboxylated latex beads of diameter $d = 0.52$ μm (IDC, Portland, USA), (2) carboxylated latex beads of diameter $d = 1.16$ μm (IDC, Portland, USA), and (3) ferromagnetic Fe_3O_4 beads of diameter $d = 1.42$ μm (provided by W. Möller, GSF, Germany). The colloidal beads were first separated from their solvent. For this purpose, suspensions were centrifuged and the pellet was resuspended in the same buffer used for the cells after the washing step. This procedure was repeated three times. To resuspend the beads from the pellet in the buffer after centrifugation the samples were first placed for 10 min in a sonicator and then further homogenized in a vortex mixer. The beads were introduced into the cells by phagocytosis. For this procedure the cell and the bead suspension were mixed, with the concentration of beads being 10 times higher than that of the cells. This mixture was placed in a rotator for 5 min. A large fraction of beads was taken up after this time. The experiments were performed immediately after the cells took up the colloidal probes and within half an hour after the phagocytosis to avoid the excretion of the probes (Rauchenberger et al. 1997).

Observation of cells by agar overlay technique

The experiments were performed by application of the established agar overlay technique (Neujahr et al. 1998) in order to facilitate the observations of the colloidal particles and to avoid long-range motion of the beads perpendicular to the cover glass and thus out of the focal plane of the objective. The setup is illustrated in Fig. 1b. The cells from the suspension were deposited on the cover glass. Immediately after removal of the buffer a small sheet was cut out of a 0.17-mm thick agar plate and deposited onto the adherent cells. In order to reduce the distance between cover glass and agar sheet, buffer was further sucked up from the intermediate space with a dry paper tissue. To avoid drying out of the adherent cells the measuring chamber was closed by a cylindrical dish (made of methacrylate) and a wet tissue was placed at the sides of the sample. The agar sheets were prepared following Yumura et al. (1984). In brief: agarose (Agar-Agar from Roth, Karlsruhe, Germany) was dissolved in phosphate buffer (3 wt%), forming a gel. The gel was melted and spread on a microscope slide. A thin film was formed by pressing a second glass plate over the spread film. The thickness of 0.17 mm was adjusted by cover slides of 0.17 mm thickness used as spacers. The agar sheets were stored in the phosphate buffer in a petri dish for up to two weeks.

Determination of velocity

The velocity of the colloidal probes in the image plane was determined by numerical differentiation according to:

$$v_{\mathrm{L}}(x_i, y_i, t_i) = \sqrt{\left(\frac{x_{i+1} - x_{i-1}}{t_{i+1} - t_{i-1}}\right)^2 + \left(\frac{y_{i+1} - y_{i-1}}{t_{i+1} - t_{i-1}}\right)^2} \qquad (2)$$

We call v_{L} the local velocity, since it shows local changes of the velocity on the smallest accessible time scale of 0.04 s. If one considers the error of the displacement and time measurements in our setup ($\Delta x = \Delta y = 10$ nm, $\Delta t = 0.04$ s), the standard deviation of v_{L} is 40%.

In order to separate long straight and short random-like parts in the trajectory we applied a method proposed by de Win et al. (1999). In this technique the distance d of two points (x_i, y_i) and (x_j, y_j) is compared with the length s of the trajectory between them. A straightness S can then be defined by the quotient:

$$S = \frac{d}{s} = \frac{\sqrt{(x_i - x_j)^2 + (y_i - y_j)^2}}{\sum_{n=j}^{i} \sqrt{(x_{n+1} - x_n)^2 + (y_{n+1} - y_n)^2}} \quad (3)$$

S varies between 0 and 1 and is a measure of the derivation of the trajectory from a straight line, for which S is equal to 1. We arbitrarily considered the trajectory as straight and as a single step if $S > 0.95$. The velocity v_S is then determined by dividing the length of the steps by the corresponding time interval. We denote v_S as the step velocity.

Results

Velocity distribution of the active motion of colloidal beads

Figure 2 shows an example of the motion of a small latex bead (diameter $d = 0.52$ μm) and of a large iron oxide bead ($d = 1.42$ μm) within a myosin II-null mutant. The total range of motion of the large and the small beads differs remarkably. Closer inspection shows that the motions appear to consist of local random walks with step widths comprising a fraction of a micrometer and nearly straight long-range motions over distances of an order of a micrometer. This is best visible for the small bead, which is first transported from the rim of the cell towards the center and then back to the rim. It is also seen that the bead is sometimes trapped within a certain region of the cytoplasm, where it performs a local (apparently random) walk (cf. right top corner of trajectory of small bead in Fig. 2). Analysis of the bead trajectories by the method of Eq. (3) shows that the motions consist of quasi-random walks with a large variation of the step width and thus exhibit typical features of Lévy flights (West and Deering 1994). This Lévy-like behavior is also reflected by the time sequence of the local velocities. In the trapped regions the step velocities are of the order 0.5 μm/s while along the long-range steps the velocities are about 1–3 μm/s. The same characteristic behavior is found also for the large beads, although the velocities of the long-range steps are smaller by about a factor of two. In order to find possible correlations between the step width and the step velocity of the bead, we plot the step velocity v_S as a function of the step widths defined in Eq. (3) for the trajectories shown in Fig. 2. As shown in Fig. 3, it is found that s and v_S are not correlated for step widths $s > 1$ μm and the velocities lie in the range 0.5–3 μm/s for the small bead ($d = 0.52$ μm) and 0.5–1.5 μm/s for the large bead ($d = 1.42$ μm). However, it is also visible that for small step widths ($0.1\ \mu m < s < 0.5\ \mu m$) the velocities increase with increasing step width. It should also be noted that bead motions and cell locomotion are not correlated within the accuracy of our measurements.

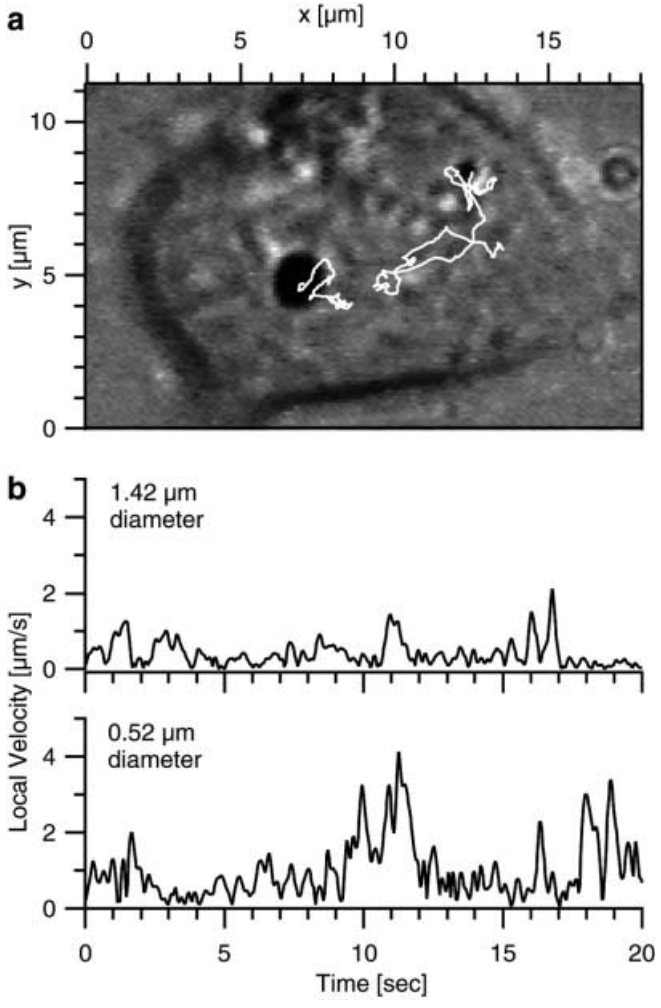

Fig. 2 **a** Trajectories of latex (diameter $d = 0.52$ μm, *right*) and iron oxide sphere ($d = 1.42$ μm, *left*) in myosin II-null mutant. Note superposition of localized random walks and directed long-range motions, which are most clearly visible for the small bead. **b** (*upper*) Local velocity of the iron oxide bead versus time; (*lower*) local velocity of the small latex sphere versus time

Another informative way to characterize the quasi-random walk of the beads is through plots of the velocity distribution function $P(v)$. In Fig. 4a the distribution functions $P(v)$ of 1.16 μm beads in wild-type cells and myosin II-null mutants are shown. Both distributions are highly asymmetric and exhibit strong tails towards high velocity. Small but pronounced differences are observed; the fraction of beads with high velocities ($v > 1.5$ μm/s) is appreciably larger for the wild-type cell than for the myosin II-null mutant, pointing to a higher apparent cytoplasmic viscosity of the latter (a point covered in the Discussion section below). In Fig. 4b we compare the distributions for beads of different diameters ($d = 0.52$ μm and $d = 1.16$ μm). It is seen that the maximum of $P(v)$ is shifted to smaller velocities for the large bead. The velocity distributions of cells adhering to glass substrates coated with BSA differ remarkably from those found for cells adhering to uncoated glass surfaces, as shown in Fig. 4c. However, the morphology of the cells on pure glass does not differ from cells on a BSA-coated substrate. The velocity distribution is strongly shifted to low velocities while the high-velocity branch is suppressed. The likely explanation is a reduction in ATP production due to the "glass effect" (Bessis 1973).

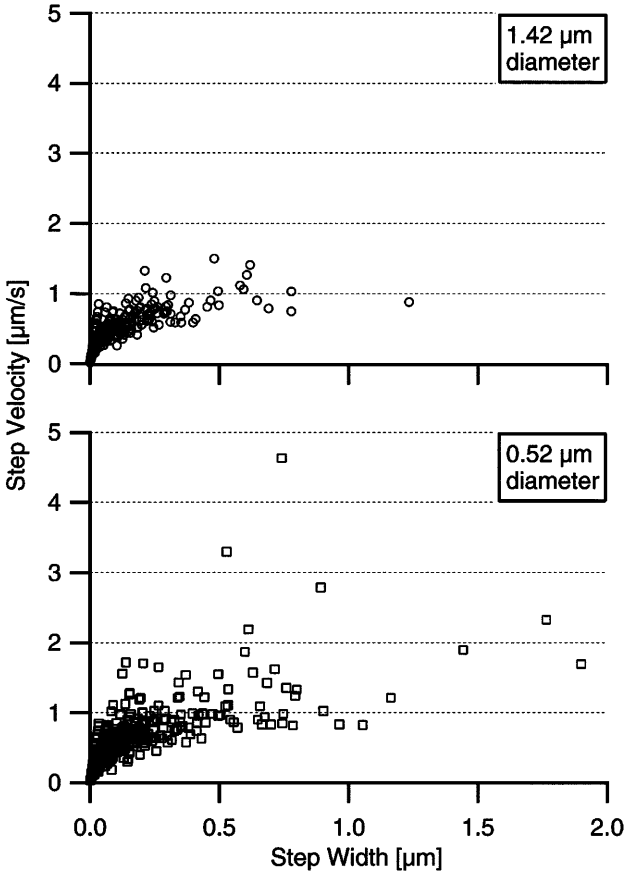

Fig. 3 Plots of step velocity versus step width determined by Eq. (3) for the two beads of Fig. 2 (1.42 µm, *top* and 0.52 µm, *bottom*)

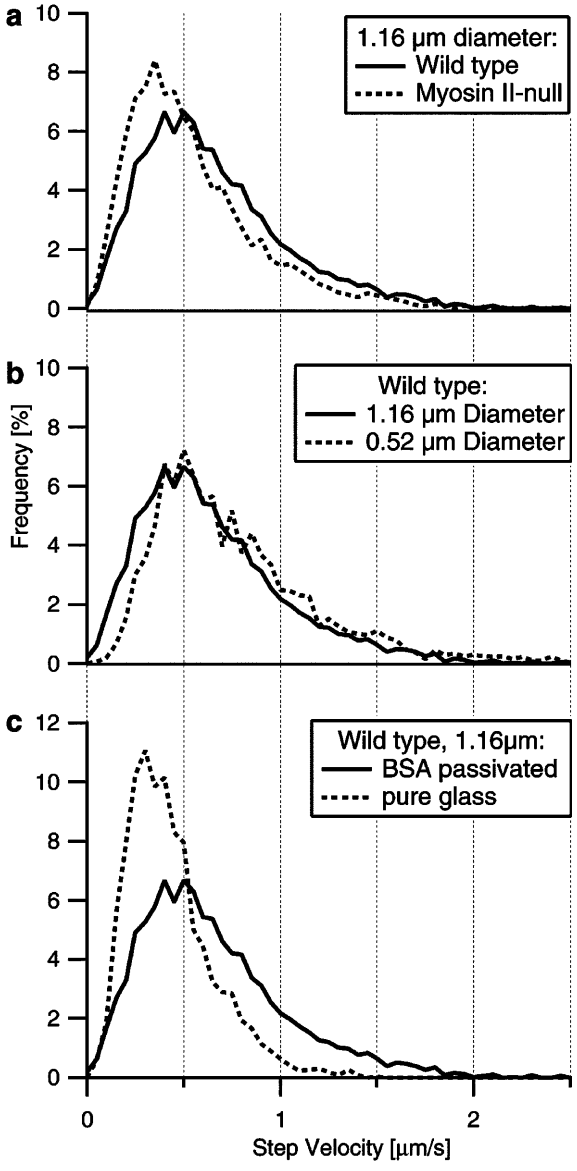

Fig. 4a–c Distribution functions $P(v)$ of the step velocity v_S. **a** Latex sphere ($d = 1.16$ µm) in wild-type (*solid line*, number of observed beads $n = 28$) and myosin II-null mutant cells (*dashed line*, $n = 37$). The cells were deposited on a BSA-coated glass surface. **b** Comparison of velocity distributions of different bead sizes, specifically 1.16 µm (*solid line*, $n = 28$) and 0.52 µm (*dashed line*, $n = 21$), in wild-type cells on BSA-coated surface. **c** Comparison of velocity distributions of 1.16 µm beads in wild-type cells on BSA-coated (*solid line*, $n = 28$) and on pure glass surfaces (*dashed line*, $n = 14$)

Micro-rheological measurements

The local viscoelastic parameters were measured by magnetic bead micro-rheology using ferromagnetic beads of diameter $d = 1.42$ µm and by applying force pulses between 50 pN and 400 pN. The viscoelastic responses induced by force pulses with 0.5–5 s duration were recorded and in many cases the modified trajectories of the beads were simultaneously analyzed. The response of the bead depends very sensitively on the applied force.

At small forces (such as 50 pN) the bead is not deflected remarkably in the force direction and the motion is largely determined by the intrinsic active transport. However, in some cases the beads were deflected with velocities of the order of 2 µm/s by the external force pulse (5 s duration) with a delay time of 2–3 s. An example of such a delayed deflection is plotted in Fig. 5a.

At large forces, that is between 200 pN and 400 pN, the beads are deflected without delay time along the field direction, typically by a few micrometers. With a few exceptions the response curves exhibit the typical shapes shown for two examples of 200 pN and 400 pN in Fig. 5b and c. The bead trajectories typically consist of an initial fast deflection which passes over (sometimes rather abruptly) into a slower motion. The deflection starts with a finite slope for all forces above 100 pN and is only partially (and sometimes barely) reversible.

This suggests that the cytoplasm of *Dictyostelium* cells does not exhibit clear elastic behavior as found, for example, for macrophages (Bausch et al. 1999). Another explanation is that the elastic regime of the cytoplasm cannot be observed when the elastic deflection length is

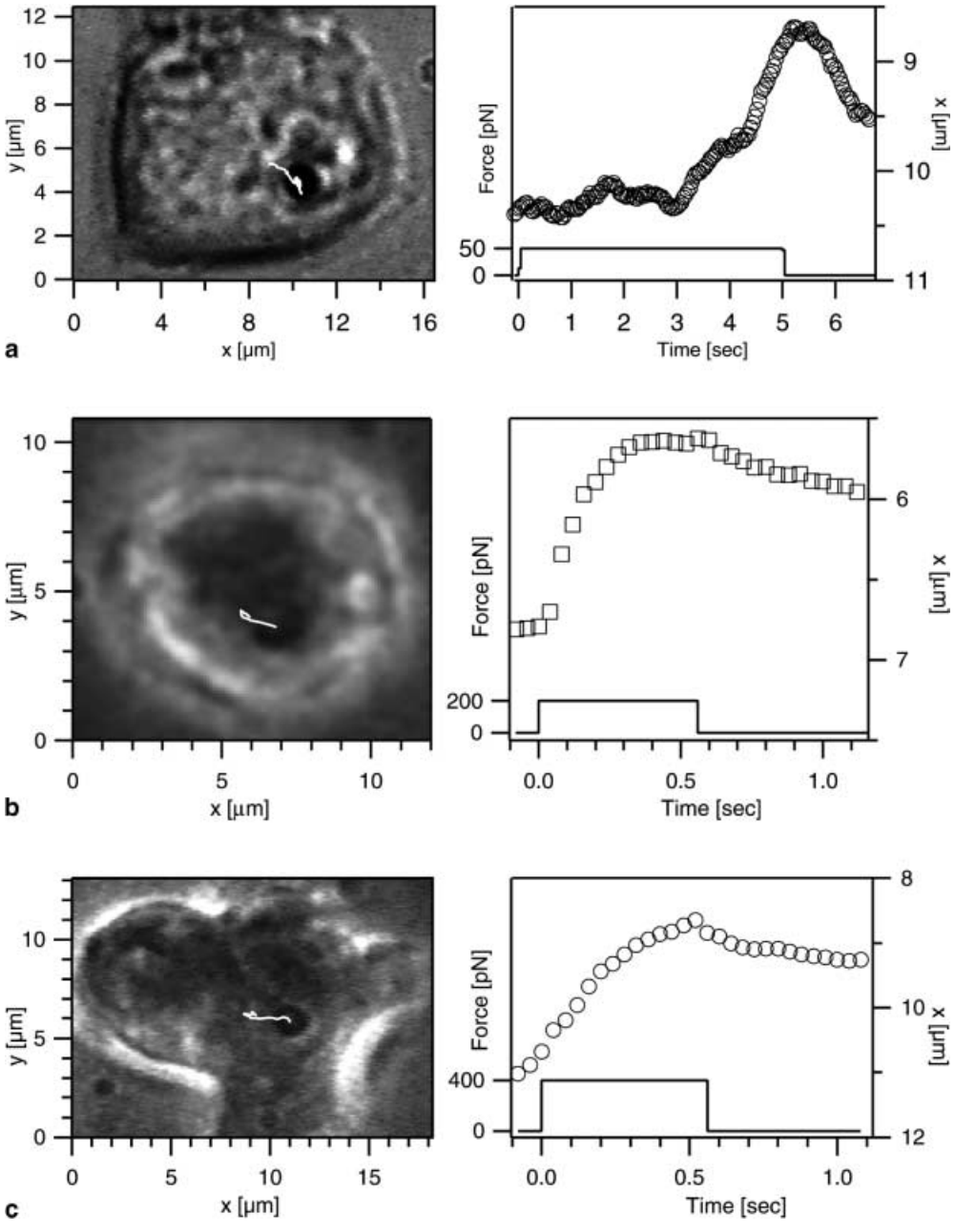

Fig. 5 **a** Deflection curve of a magnetic bead of diameter $d = 1.42$ μm under the influence of a force pulse of 50 pN of 5 s duration. **b** Typical viscoelastic response curve of a magnetic bead of diameter $d = 1.42$ μm induced by force pulses of $F = 200$ pN. **c** Typical viscoelastic response curve of a magnetic bead of diameter $d = 1.42$ μm induced by force pulses of $F = 400$ pN. On the *left-hand side* the trajectories are visualized. The *right-hand side* shows plots of the deflection of the particle versus time. The pulses are marked by the square wave. Note: the force is applied to the negative x-axis; the bead deflection under the influence of the external force is thus negative

smaller than the step widths of active bead motion driven by the internal dynamics of the network. Some evidence for this view is provided by the finding that for very short pulses (duration < 0.1 s) the bead trajectories are in most cases reversible, although the response curve exhibits a finite slope.

Despite the complexity of the viscoelastic response curves, it is useful to analyze the curves in terms of the mechanical equivalent circuit to determine effective viscoelastic parameters as a quantitative measure of the viscoelasticity of the cytoskeleton in order to compare data of different cells. The response curves can most conveniently be analyzed by the circuit shown in Fig. 6, which consists of a dashpot (η_D) in series with a so-called Voigt element, a parallel circuit of a spring (μ_V) and a second dashpot (η_V). η_V accounts for the finite initial flow of the bead and the entire Voigt element for the saturation behavior of the initial deflection. For long times $t > \tau_V = \eta_V/\mu_V$, only the viscosity η_D determines the long-range displacement. The creep compliance of the equivalent model under the influence of an external force is described by the following equation:

$$J(t) = \frac{1}{\mu_V}\left(1 - e^{-\frac{t}{\tau_V}}\right) + \frac{1}{\eta_D}t\,, \tag{4}$$

where τ_V is the relaxation time characterizing the transition into the saturation state. Values of the viscosity η_D and the elastic modulus μ_V measured for forces of 140,

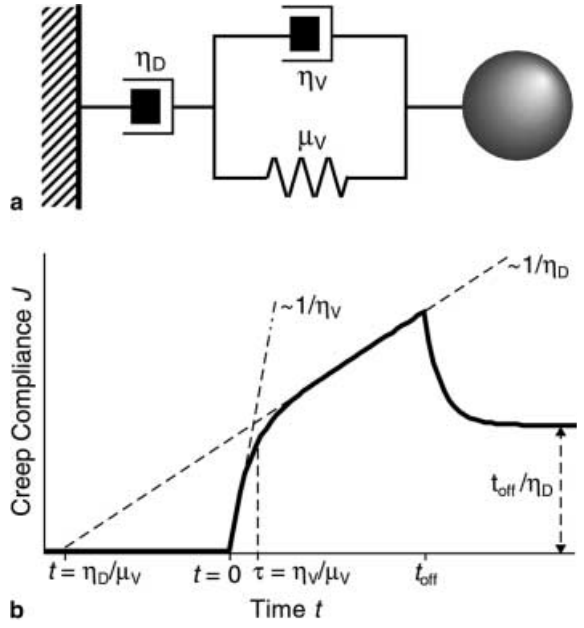

Fig. 6a, b Mechanical equivalent circuit enabling formal analysis of creep response and recovery curves in terms of apparent viscosities and elastic moduli. **a** Mechanical model consisting of a Voigt body (V) and a dashpot (D) in series. **b** Theoretical creep response and recovery curve of the mechanical equivalent circuit

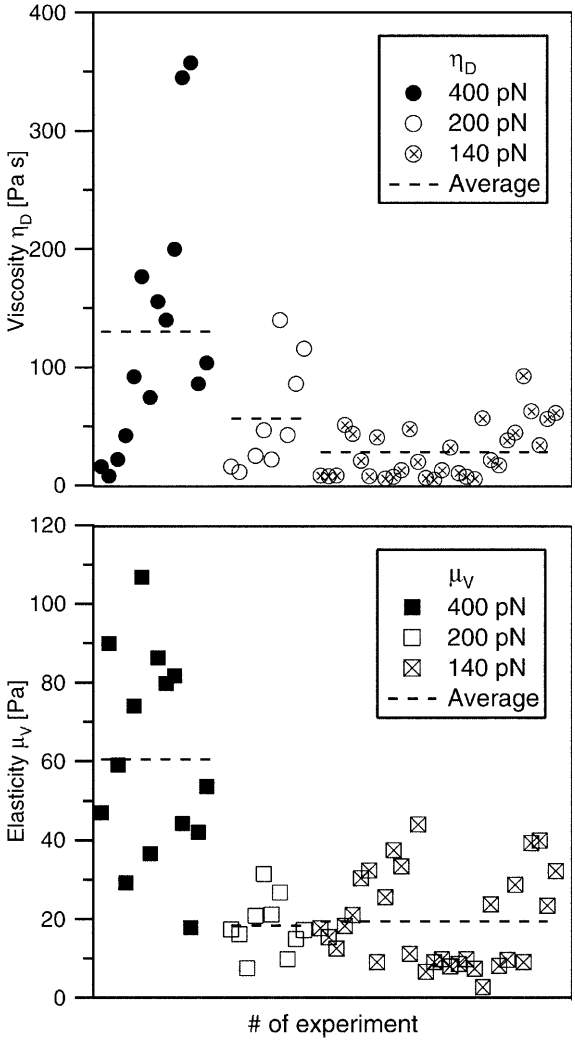

Fig. 7 The viscoelastic parameters η_D (*upper*) and μ_V (*lower*) of all observed cells for the forces 140, 200, and 400 pN. The *dotted lines* indicate the average value for each force

200, and 400 pN are plotted in Fig. 7. For the two lower forces the viscosities η_D vary between 10 Pa s and 100 Pa s with an average of $\langle\eta_D\rangle = 40$ Pa s, while for the large force many values of η_D lie in the same range as those measured for the weaker forces, but they extend up to 350 Pa s. Similar behavior is found for the elastic modulus.

This complex, force-dependent viscoelastic response can be explained in terms of viscoplastic behavior of the cytoplasm. That is, by assuming that the force-induced motion of the magnetosomes over distances of the order of a micrometer is determined by the fracture of local bonds within the cytoplasmic scaffold at forces exceeding the local yield stress. Thus the local yield stress varies at least from 30 Pa (corresponding to forces of 50 pN for 1.42 μm beads) to 250 Pa (corresponding to 400 pN for 1.42 μm beads). Further evidence for this interpretation is provided by the observation of the bead trajectories. For 400 pN the paths are in most cases straight lines (see Fig. 5), while for 200 pN the bead trajectories sometimes exhibit a bend before saturation starts and the bead velocity decreases abruptly. This is most likely due to the fact that the bead is deflected by a rigid obstacle while the stress is below the threshold value σ^* required to open a path in the more rigid region of the cytoplasm. Evidence for this view is provided by the finding that the decreased velocity along the deflected trajectories agrees reasonably well with the value expected for the force component along this path.

Estimation of active forces

We attempt to measure the active force F_{act} on the beads moving along the microtubuli by analyzing the change in direction and speed of motion caused by an external force pulse as shown in Fig. 8. We chose trajectories of beads exhibiting the following scenario. Before application of the external force the bead moves with speed v_1 at an angle ϑ_1 with respect to the force direction. After application of the force pulse the angle changes to ϑ_2 and the speed changes to v_2. The velocity in the presence of the external force F_{mag} is:

$$v_2 \cos\vartheta_2 = v_1 \cos\vartheta_1 + \frac{F_{mag}}{\zeta} \tag{5}$$

where ζ is the friction coefficient, which is related to the viscosity η_D by $\zeta = 6\pi\eta_D a$, where a is the radius of the bead. The unknown local friction coefficient can now be eliminated (by assuming that ζ is the same before and

after application of the pulse) by $\zeta = F_{act}/v_1$. The unknown active force is then obtained by the equation:

$$F_{\mathrm{act}} = \frac{v_1}{v_2 \cos\vartheta_2 - v_1 \cos\vartheta_1} F_{\mathrm{mag}} \qquad (6)$$

Since F_{mag} is known, F_{act} can be determined by measuring v_1, v_2, $\cos\vartheta_1$, and $\cos\vartheta_2$. Consider the example of Fig. 8, in particular pulse number 2. The initial velocity is about $v = 0.6$ μm/s and the trajectory forms an angle $\vartheta_1 = 60°$ with the ordinate. The velocity in the direction of the force ($\vartheta_2 = 0$) is $v_2 = 1.1$ μm/s. We thus find $F_{\mathrm{act}} = 100$ pN.

A rough estimate is also obtained from the measurements of the velocity distributions and the cytoplasm viscosity η_{D} through micro-rheometry. According to the experiments at $F = 140$ pN and $F = 200$ pN, the average viscosity of the cytoplasm is 40 Pa s. The average velocity of the beads of $d = 1.16$ μm diameter is about 0.5 μm/s. Thus we find $F_{\mathrm{act}} = 6\pi\eta_{\mathrm{D}} av = 200$ pN.

Discussion

Heterogeneous viscoelasticity of the cytoplasm

One major purpose of the present study was to demonstrate the application of the colloidal probe technique in combination with magnetic bead micro-rheology for the measurement of velocity distributions of the intracellular transport of internalized particles and for the measurement of active forces. The colloidal beads are taken up by the cell via phagocytosis. These phagosomes are thus enclosed in a membrane derived from the cell envelope. Their exposed surfaces resemble initially the inner leaflet of the plasma membrane, exhibiting in addition membrane-associated elements of the actin cortex and in particular the actin-binding protein coronin. Following Maniak et al. (1995), these residues of the actin cortex are gradually released from the phagosomes within 1 min after engulfment and the particles are transported alternately from the periphery of the cell to the center and back along the microtubuli, as shown for instance in Fig. 2. The transport to the centrosome is generally attributed to dynein and that to the periphery to kinesin (Alberts et al. 1994).

As will be discussed in the following, our experimental findings can be well explained by assuming that the cytoplasm of *Dictyostelium* cells behaves as a viscoplastic body. The motion of the particles is mainly determined by the rate of fracture of bonds within the intracellular scaffold. This network is mainly composed of the cytoskeleton components actin and microtubuli with their associated regulation proteins. However, it is well possible that also the network-like assembly of the osmoregulatory organelle composed of cisternae and interconnecting ducts contributes to the viscoelasticity of the cytoplasm. In this model the space-dependent viscoelastic compliance $J(r, t)$ is a measure of the local mobility $\mu(r)$ according to $v(r) = \mu(r)F_0$ (Ziemann et al. 1994). The mobility $\mu(r)$, and therefore also the reciprocal of the apparent viscosity η_{D}, is determined by the rate of fracture of bonds which is, however, force dependent (see Fig. 7).

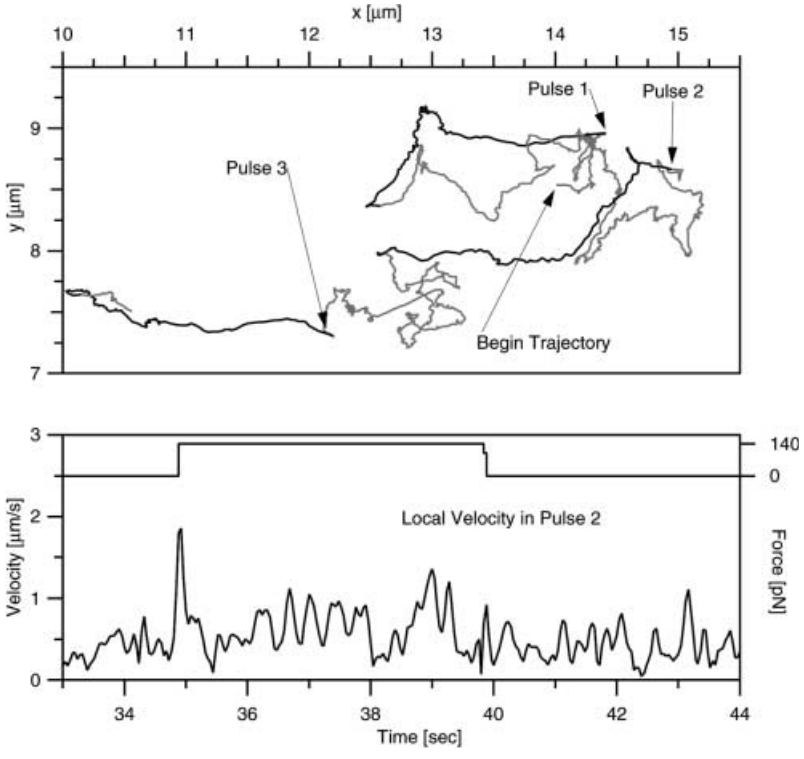

Fig. 8 (*upper*) Trajectory of a bead subjected to three force pulses of 140 pN at high resolution. The onset of the pulses are drawn *black*, the trajectories between the pulses are *gray*. The force is applied in the negative *x*-direction. Note in particular the deflection at the end of pulse 1 and at the beginning of pulse 2. (*lower*) Step velocity during pulse 2

The analysis of a large number of trajectories showed that the internalized beads perform quasi-random walks consisting of straight long-range motions extending over micrometer distances and local random walks with step widths of the order of 0.1 μm. The local motion of the beads is most likely due to the intrinsic dynamics of the cytoplasm. One possibility, for instance, is the pronounced bending fluctuations of the microtubuli to which the beads are attached. In fact, separate observations of these bending fluctuations by fluorescence studies of cells with GFP-labeled microtubuli showed that the maximum velocities of the transverse wobbling motion of the filaments lie indeed in the range of 0.2 μm/s.

The step velocities v_S along the long-range trajectories depend on the diameter of the phagosomes. For $d = 0.52$ μm we find $1\ \mu m/s < v_S < 3\ \mu m/s$ and for $d = 1.42$ μm beads then $0.5\ \mu m/s < v_S < 1.5\ \mu m/s$. The maximum bead velocity thus decreases with increasing bead size. We attribute this motion to the transport along the microtubuli, which implies that the total transport force does not depend on the bead size. The velocities of the short-range motions extend from 0 to 0.8 μm/s, with a maximum at approximately 0.5 μm/s, and do not depend appreciably on the bead size.

The main evidence for the viscoplastic model comes from the strong force dependence of the trajectories of the magnetosomes. At large forces ($F_{mag} = 400$ pN) the beads are in most cases deflected along straight lines in the direction of the force (see Fig. 5c), since the applied stress is larger than the yield stress of the mechanically hard and soft regions of the cytoplasm. At intermediate force pulses ($F_{mag} = 100$–200 pN) the beads are deflected in the direction of the force with high velocity, but are then deflected in a different direction, moving with slower velocity (see Fig. 8). An explanation for this behavior is that the bead encounters a region exhibiting a higher yield stress than that generated by the force amplitude F_{mag} and moves along the surface of this hard region. The velocity is reduced, since the acting force is reduced to $F = Fcos\alpha$, where α is the angle of the deflection.

At low forces ($F_{mag} < 100$ pN) the beads are in general not deflected immediately after application of the force F_{mag} and their motion is dominated by the active processes of the cell. However, the beads are often deflected in the field direction with high velocity (2 μm/s at $F_{mag} = 50$ pN) after a time delay of several seconds. This leads to the conclusion that the beads are trapped in a hard region from which they escape slowly under the action of the applied force, as discussed in more detail below.

Judged from the measurement of the distributions of apparent viscosities (summarized in Fig. 7), the cytoplasm seems to exhibit rather soft regions characterized by viscosities as low as 5 Pa s and hard clusters exhibiting apparent viscosities of several hundred Pa s. In the soft regions the magnetosomes can be transported with velocities of more than 2 μm/s by a force of 50 pN along long-range paths. The yield force of the hard regions is of the order of 400 pN, which cannot be penetrated rapidly by the magnetosomes subjected to active forces (~100 pN).

Dynamic nature of the yield force

The finding that at low external forces the beads may escape a region of high mechanical strength (exhibiting a yield stress large compared to the applied stress), with time delays of a few seconds, shows that the yield stress is a dynamic quantity which is expected to depend on the rate of force application. The reason for this is that local cross-links within the cytoplasmic network break statistically. The probability k per unit time to break a single bond depends on the force according to the modified Arrhenius-Kramers law:

$$k = k_0 \exp\left[-\frac{\Delta g - F_0\xi}{k_B T}\right] \tag{7}$$

where Δg is the activation energy of a single bond breakage and $F_0\xi$ is the work performed by the (unknown) local force acting on the bond considered; ξ is the mesh size if we consider the cytoplasm as a network.

The dynamic nature of unbinding forces between single biomolecules has been systematically studied over recent years by nanomechanical techniques and these studies showed that the behavior is well described by the Arrhenius-Kramers theory (Merkel et al. 1999; Simson et al. 1999). Similar considerations have been applied to explain the temperature dependence of the plastic deformation of technical materials. Following the above considerations, the velocity of the beads is related to the local shear stress σ_L generated by the beads as:

$$v \sim \exp\left[-\frac{\Delta G - V\sigma_L}{k_B T}\right] \tag{8}$$

Since several cross links have to be broken in order to enable the bead to move by a distance of the order of the mesh size ξ, ΔG is the sum of the activation energies of all bonds (to be broken); V is the so-called strain volume, which is expected to be of the order of the third power of the mesh size ξ^3; σ_L is the local stress applied by the bead.

Equation (8) provides a general scheme for the evaluation of the viscoelastic parameters in terms of the molecular structure and the bond strength of the cytoplasmic networks. It contains several unknown physical parameters, notably V and ΔG. Nevertheless, local measurements of the force-induced bead velocities allow us to characterize the local mechanical strength of the cytoplasm in a quantitative way. Useful applications of this scheme are the measurement of active forces and the quantitative characterization of the modification of the mechanical strength by mutations.

The unknown parameter ΔG may be eliminated by comparing the velocities evoked by different force

amplitudes (or stresses σ). Thus Eq. (8) yields for the ratio of velocities v_1/v_2 induced by forces $F_{mag,1}$ and $F_{mag,2}$:

$$V(\sigma_1 - \sigma_2) = k_B T \ln(v_1/v_2) \quad (9)$$

For $F_{mag,1} = 140$ pN and $F_{mag,2} = 100$ pN we find $v_1/v_2 \approx 2$, and with $\sigma = F/(\pi a^2)$ one finds for the strain volume $V = 2.4 \times 10^{-21}$ m^3 or $\xi \approx 0.1$ μm.

Facilitated and delayed transport of phagosomes

Our micro-mechanical study shows that the apparent viscoelastic moduli of the cytoplasm of *Dictyostelium* cells vary by at least one order of magnitude. It seems to be composed of both mechanically soft and hard regions. The soft regions exhibit apparent viscosities below 10 Pa s (see Fig. 7). Phagosomes can be transported within these regions over long distances by relatively weak forces of 50 pN with velocities in the range of 1 μm/s. These regions thus appear to behave as viscous fluids within which phagosomes can be rapidly transported by external forces of 100 pN or smaller. The mechanical hard regions behave as viscoplastic bodies, exhibiting yield stresses of the order of a few 100 Pa. The transport velocity of phagosomes through these regions is determined by the rate of fracture of bonds (most likely of cross-links within the actin- and microtubuli-based cytoskeleton). The active forces (of about 100 pN or less) can generate stresses of the order of $\sigma_{act} = 60$ Pa and they are thus too weak to transport phagosomes through the hard region with high velocity (> 1 μm/s). However, our study showed that the yield stress is a dynamic quantity, since the rate of fracture of cross-links is determined by the modified Arrhenius-Kramers law and can increase exponentially with the local stress generated by the active force. The active transport of the magnetosomes along the microtubuli is thus slowed down by the hard regions of the cytoplasm but not completely hindered, since the constant force can lead to a slow dissolution of the hard network in front of the transported particles according to Eq. (8). The transport of the beads through the hard regions is expected to be further facilitated by the rupture of bonds by the random active forces driving the local random walk of the beads or the wobbling motion of the microtubuli. Such wobbling has been observed in separate experiments (W. Feneberg, unpublished data) and is expected to be caused by active forces exerted along the entire length of the filament.

Effect of myosin II deficit

The velocity distributions of the random walks in wild-type cells and myosin II-null mutants differ appreciably. The maxima of the normalized distributions are higher for the mutant, which holds for both sizes of beads ($d = 0.52$ μm and $d = 1.16$ μm). The higher maximum in the distribution may be interpreted in terms of greater sharpness of the distribution of the random motion. The high-speed tails of the larger beads are remarkably smaller for the mutant. Since the bead velocity is determined by the apparent local viscosity η_D of the cytoplasm, this change in $P(v)$ strongly suggests that the apparent viscosity of the mutants lacking myosin II is on the average higher. This is in good agreement with a recent study of the viscoplastic behavior of the envelope of *Dictyostelium* cells by the micropipette aspiration technique (Merkel et al. 2000). In this work it was shown that the cell membrane is disrupted from the main body of the actin cortex and aspirated by the pipette above a threshold pressure, enabling measurements of the actin cortex-membrane coupling strength in terms of the yield force. It was shown that the yield force at which cell protrusion flows into pipettes is considerably larger for the myosin II-null mutant than for the wild type. A likely explanation for this and the present finding is that the lack of myosin II is compensated by an increase of the activity or concentration of other cross-linkers present in *Dictyostelium* cells (such as α-actinin and the 120 kDa gelation factor). Since myosin II is a highly dynamic cross-linker exhibiting a rapid association-dissociation equilibrium in the presence of ATP while the off-rate of the actin binding of other cross-linkers is much slower, the yield force is expected to be indeed higher for myosin II-null mutants.

Effect of substrate

A pronounced difference is found between the behavior of cells adhering on untreated glass surfaces and on BSA-coated surfaces. The high velocity tails are strongly reduced on pure glass. Again the effect is more pronounced for myosin II-null mutants than for wild-type cells. The most likely explanation for this finding is again a higher effective viscosity of the cytoplasm. We do not have an explanation for this increase of the mechanical strength due to the contact of the cells with pure glass surfaces. One possible explanation is that the adhesion strength of the cells on pure glass is higher than on BSA-coated substrates and some evidence for this view was provided previously (Schindl et al. 1995). The cells could avoid a too strong flattening on substrates exhibiting a strong adhesion force in an interactive way by increasing the mechanical strength of the cytoplasm.

Acknowledgements This work was supported by the Deutsche Forschungsgemeinschaft (SFB 266) and the Fonds der Chemischen Industry. We greatly acknowledge many enlightening discussions with G. Gerisch (MPI für Biochemie). We also thank W. Möller (GSF, Munich) for his gift of ferromagnetic beads.

References

Alberts B, Bray D, Lewis J, Raff M, Roberts K, Watson JD (1994) Molecular biology of the cell. Garland, New York

Bausch AR, Ziemann F, Boulbitch A, Jacobson K, Sackmann E (1998) Local measurements of viscoelastic parameters of adherent cell membranes by magnetic bead microrheometry. Biophys J 75:2038–2049

Bausch AR, Möller W, Sackmann E (1999) Measurements of local viscoelasticity and forces in living cells by magnetic tweezers. Biophys J 76:573–579

Bessis M (1973) Living blood cells and their ultrastructures. Springer, Berlin Heidelberg New York

Janmey P (1995) Cell membrane and the cytoskeleton. In: Lipowski R, Sackmann E (eds) Handbook of biological physics. Elsevier, Amsterdam, pp 805–849

Kolodney ME, Elson EL (1993) Correlation of myosin light chain phosphorylation with isometric contraction of fibroblasts. J Biol Chem 268:23850–23855

Maniak M, Rauchenberger R, Albrecht R, Murphy J, Gerisch G (1995) Coronin involved in phagocytosis: dynamics of particle-induced relocalization visualized by a green fluorescent protein tag. Cell 83:915–924

Manstein DJ, Titus MA, Lozanne AD, Spudich JA (1989). Gene replacement in dictyostelium: generation of myosin null mutants. EMBO J 8:923–932

Merkel R, Nassoy P, Leung A, Ritchie K, Evans E (1999) Energy landscapes of receptor-ligand bonds explored with dynamic force spectroscopy. Nature 397:50–53

Merkel R, Simson R, Simson DA, Hohenadl M, Boulbitch A, Wallraff E, Sackmann E (2000) A micromechanic study of cell polarity and plasma membrane cell body coupling in dictyostelium. Biophys J 79:707–719

Neuhäuser H, Schwink C (1993) Solid solution strengthening. In: Mughrabi H (ed) Plastic deformation and fracture of materials. VCH, New York, pp 191–250

Neujahr R, Albrecht R, Köhler J, Matzner M, Schwartz J-M, Westphal M, Gerisch G (1998) Microtubule-mediated centrosome motility and the positioning of cleavage furrows in multinucleate myosin II-null cells. J Cell Sci 111:1227–1240

Pawson T, Scott JD (1997) Signaling through scaffold, anchoring, and adaptor proteins. Science 278:2075–2080

Rauchenberger R, Hacker U, Murphy J, Niewöhner J, Maniak M (1997) Coronon and vacuolin identify consecutive stages of a late, actincoated endocytic compartment in *dictyostelium discoideum*. Curr Biol 7:215–218

Raucher D, Stauffer T, Chen W, Shen K, Guo S, York JD, Sheetz MP, Meyer T (2000) Phosphatidylinositol 4,5-bisphosphate functions as a second messenger that regulates cytoskeleton-plasma membrane adhesion. Cell 100:221–228

Schindl M, Wallraff E, Deubzer B, Witke W, Gerisch G, Sackmann E (1995) Cell-substrate interactions and locomotion of dictyostelium wild-type and mutants defective in three cytoskeletal proteins: a study using quantitative reflection interference contrast microscopy. Biophys J 68:1177–1190

Schmidt FG, Ziemann F, Sackmann E (1996) Shear field mapping in actin networks by using magnetic tweezers. Eur Biophys J 24:348–353

Simson DA, Strigl M, Hohenadl M, Merkel R (1999) Statistical breakage of single protein A-IgG bonds reveals crossover from spontaneous to force-induced bond dissociation. Phys Rev Lett 83:652–655

Small JV, Rottner U, Kaverina I (1999) Functional design in the actin cytoskeleton. Curr Opin Cell Biol 11:54–60

West BJ, Deering W (1994) Fractal physiology for physicists: Lévy statistics. Phys Rep 246:1–100

Win AHN de, Pierson ES, Derksen J (1999) Rational analyses of organelle trajectories in tobacco pollen tubes reveal characteristics of the actomyosin cytoskeleton. Biophys J 76:1648–1658

Yumura S, Mori H, Fukui Y (1984) Localization of actin and myosin for the study of amoeboid movement in dictyostelium using improved immunofluorescence. J Cell Biol 99:894–899

Ziemann F, Rädler J, Sackmann E (1994) Local measurements of viscoelastic moduli of entangled actin networks using an oscillating magnetic bead rheometer. Biophys J 66:2210–2216